Kinesin Family Member 12 Is a Candidate Polycystic Kidney Disease Modifier in the *cpk* Mouse

Michal Mrug,* Renhua Li,[§] Xiangqin Cui,[§] Trenton R. Schoeb,[†] Gary A. Churchill,[§] and Lisa M. Guay-Woodford*[†‡]

*Departments of *Medicine, [†]Genetics, and [‡]Pediatrics University of Alabama at Birmingham, Birmingham, Alabama; and [§]The Jackson Laboratory, Bar Harbor, Maine*

The *cpk* mouse is the most extensively characterized model of autosomal recessive polycystic kidney disease (ARPKD). The major ARPKD-related renal and biliary phenotypes are modulated in F2 mutants by genetic background, suggesting that quantitative trait loci (QTL) modulate disease severity. In 461 F2 *cpk* mice, kidney length, weight, and volume were scored as quantitative traits (QT), and a semiquantitative method to assess biliary duct number, area (BDA), portal vein area, and total area of each portal field, as well as the severity of cholangitis, was developed. QTL mapping was performed with Pseudomarker v1.02. Candidate genes were identified within the QTL intervals on the basis of expression profiling, reverse transcriptase–PCR, haplotypes, and sequence analysis. The renal QT were normally distributed in the F2 cohort and strongly correlated ($P < 0.001$). Among the biliary QT, only BDA correlated with the renal QT ($P < 0.01$). Genome-wide scan identified a major effect QTL on chromosome (Chr) 4 for the renal traits, adjusted BDA, and cholangitis with logarithm of odds scores of 18, 8, and 5, respectively. Regression modeling refined the Chr 4 main effect into an approximately 50-cM region with three distinct QTL peaks at 16, 34, and 54 cM. *Kif12*, a gene encoding a novel kinesin, mapped beneath the 34 cM QTL peak and has expression level variants and strain-specific sequences that were associated with renal disease severity in affected mice. Therefore, the positional candidate gene, *Kif12*, fulfills the major criteria for QTL gene discovery established by the Complex Trait Consortium, and, thus, it is proposed that *Kif12* is a *cpk* modifier gene.

J Am Soc Nephrol 16: 905-916, 2005. doi: 10.1681/ASN.2004121083

Polycystic kidney disease (PKD) is one of the most common genetic disorders, affecting >600,000 people in the United States, and is a major cause of ESRD in children and adults (1). Autosomal dominant PKD (ADPKD; MIM 173900; 173910) occurs in 1:400 to 1:1000 individuals and is caused by mutations in one of two genes, *PKD1* or *PKD2* (2–5). Autosomal recessive PKD (ARPKD; MIM 263200) is less frequent (1:20,000 live births) and occurs as a result of defects in a single gene, *PKHD1* (6,7). In both disorders, interfamilial and intrafamilial phenotypic variability is observed (8,9), the latter suggesting that variation at nondisease (modifier) loci may modulate disease expression.

Given the genetic complexity of human populations, efforts to identify modifier genes or quantitative trait loci (QTL) in single-gene disorders have largely focused on experimental models. Numerous murine (mouse and rat) PKD models have been described in which the mutant phenotypes closely resemble human PKD with respect to cyst morphology, cellular and extracellular matrix abnormalities, and disease progression (reviewed in 10). Mapping strategies have identified several putative QTL intervals in experimental crosses segregating different PKD gene mutations. Of note, proximal chromosome (Chr) 4 reportedly harbors putative modifying gene(s) for the renal cystic disease expressed in the *cpk*, *bpk*, *jck*, and *pcy* models (11–14). To date, however, the specific genetic variants underlying this or any other major effect PKD QTL have yet to be identified.

With respect to PKD experimental models, the *cpk* mouse is one of the most extensively characterized (15,16). The *cpk* mutation (*cpk* or *Cys1*^{cpk}) arose spontaneously in the C57BL/6J-Pldn^{Pa} (B6) strain, and the *Cys1*^{cpk} allele involves a tandem deletion that is predicted to cause truncation of the novel, cilia-associated protein, cystin (17,18). In *cpk* mutants, disease expression and severity are modulated by genetic background (11,19). The renal phenotype is dominated by massive cystic involvement of the collecting ducts, a pattern that strongly resembles human ARPKD (20). In the liver, the ductal plate malformation (DPM) gives rise to a biliary dysgenesis lesion that is similar to ARPKD-related congenital hepatic fibrosis (CHF). Although this biliary phenotype is not observed in B6-*cpk/cpk* mice (16), it is fully penetrant and variable when *Cys1*^{cpk} is expressed in crosses with other strains, *e.g.*, *Mus mus castaneus* (CAST/Ei), DBA/2J, BALB/c, or CD1 (19,21–23).

In the current study, we examined both the *cpk*-associated renal and biliary phenotypes as sets of quantitative traits (QT). Consistent with recent observations in human ARPKD cohorts (9), we observed that in our *cpk* cross, the severity of the renal

Received December 14, 2004. Accepted January 5, 2005.

Published online ahead of print. Publication date available at www.jasn.org.

Address correspondence to: Dr. Lisa M. Guay-Woodford, Division of Genetic and Translational Medicine, University of Alabama at Birmingham, 740 Kaul Human Genetics Building, 720 20th Street South, Birmingham, AL 35294. Phone: 205-934-7308; Fax: 205-975-5689; E-mail: lgw@uab.edu

ISSN: 1046-6673/1604-0905

and biliary disease was only weakly correlated. Genome scanning identified a major effect QTL complex on Chr 4 that modulates the renal cystic disease, components of the biliary lesion, and cholangitis. Gene expression analyses suggest that variations in *Kif12*, the gene encoding a novel kinesin, underlie the Chr 4 main effect on the renal and biliary phenotypes.

Materials and Methods

Mice

Mice that were used in these experiments were bred from stock colonies of C57BL/6J-+/*cpk* (B6-+/*cpk*) mice and CAST/Ei (CAST) mice maintained at the University of Alabama at Birmingham. F1 progeny heterozygous for the *Cys1*^{cpk} allele were identified using an allele-specific assay (17) and intercrossed to generate F2 mutants. All F2 mice were killed 10 d after birth. One kidney and the right liver lobe were fixed in 10% buffered formalin, embedded in paraffin, and analyzed using standard histologic methods. The remaining kidney and liver were snap-frozen and stored in liquid nitrogen. The *cpk* genotype was confirmed by PCR with DNA prepared from spleens using standard procedures. All protocols were approved by the University of Alabama at Birmingham Animal Care and Use Committee. The University of Alabama at Birmingham is fully accredited by the American Association of the Accreditation of Laboratory Animal Care.

Phenotypic Characterization

The following parameters were measured in the F2 kidneys: Kidney length (KL), kidney weight (KW), kidney volume (Kvol; measured by water displacement), crown to rump length (CR), and body weight (BW). In addition, we calculated the commonly used ratios KL/CR and KW/BW.

In the liver, the DPM associated with human ARPKD is characterized by three key features: (*1*) "chaotic" branching and dilation of the bile ductules, (*2*) biliary epithelial hyperplasia, and (*3*) immature stroma and fibrosis within the portal triad (24). Therefore, we designed a semiquantitative, histopathologic scoring system and used digital imaging to assess the peripheral portal triads for the following: (*1*) the number of bile ducts/ductules per portal vein (BDN; an index of ductal branching), (*2*) the bile duct area (BDA), (*3*) the portal vein area (PVA), and (*4*) the total area of the portal tract (TOTA). We also computed the ratio BDA/PVA to "normalize" the trait for area distortions that can occur when cutting tubular structures in cross-section. A minimum of two portal triads were analyzed per section with two or more sections evaluated per liver.

In addition, we scored the cholangitis severity using a five-point system that assessed the extent of inflammatory cell infiltrate around the biliary ducts and in the liver parenchyma, as well as the degree of biliary ductal changes ranging from epithelia hyperplasia to epithelial necrosis. According to this scoring system, "0" represented no/minimal inflammation and "4" reflected severe and extensive cholangiohepatitis.

Images were acquired using a Nikon E600 microscope equipped with a SPOT Insight digital camera (Diagnostic Instruments, Sterling Heights, MI). Image analyses were performed with Sigma Scan Pro v5 image analysis software (SPSS Inc., Chicago, IL). Statistical evaluations of the phenotypic data, including trait distributions and correlations, were performed with SPSS 11.5 statistical software package (SPSS Inc.).

PCR-Based Genotyping

Microsatellite markers from Whitehead/MIT Genome Database (http://www-genome.wi.mit.edu) that were spaced at approximately 25-cM intervals throughout the genome and whose B6 and CAST alleles differed by at least 10 bp were typed by PCR and resolved on agarose gels using standard methods. When the initial genome scan identified a major effect QTL on Chr 4, additional typing was performed with markers spaced at approximately 10-cM intervals along the chromosome. Primers were purchased from Research Genetics (MapPairs, Huntsville, AL). Primer information is available upon request.

Single-nucleotide polymorphisms (SNP) within the *Kif12* gene were identified from the Celera Mouse SNP Database (http://myscience.appliedbiosystems.com/servlet/com.celera.web.cds_servlets. [mouse_refsnp-Gene_ID]). Primers NT_039262(Kif12)-1245F (5′-TTAGTGCTCCGCAAAGAAGC-3′) and NT_039262(Kif12)-1643R (5′-TTCCACATAGAAGCCTCGTG-3′) amplified a 398-bp product that included SNP mCV24480597. Primers NT_039262(Kif12)-2867F (5′GGGCTAGAGTTCTGGCATCA-3′) and NT_039262(Kif12)-3266R (5′CTGCTGCAAGAGCAGGAAG-3′) amplified a 399-bp product that included SNP mCV24480596 and mCV24480595. Primers NT_039262(Kif12)-4222F (5′-ACACCACGGGTATGAGCTTC-3′) and NT_039262(Kif12)-4756R (5′-CTGAAGCCAATGATCAGACG-3′) amplified a 534-bp product that included SNP mCV24480588. Primers NT_039262(Kif12)-5638F (5′-AGGCCCCAGGTCACATATC-3′) and NT_039262(Kif12)-6078R (5′-TACCCTTTCCCCAAGTTTCC-3′) amplified a 440-bp product that included SNP mCV24480587. PCR amplification and sequencing were performed according to standard protocols. Primers NT_039262(Kif12)-4222F and NT_039262(Kif12)-4756R were specific for the B6 allele, and no amplification product was detected for the CAST allele.

QTL Mapping

QTL analyses were performed with the Pseudomarker software package (release 1.02; http://www.jax.org/staff/churchill/labsite) using the method for genome-wide scans developed by Sen and Churchill (25). Genome-wide significance thresholds were determined by permutation testing for each trait (26). Significant or suggestive QTL meet or exceed the 95 and 37% genome-wide thresholds, respectively. Confidence intervals (CI) were determined by computing the region of the posterior density curve that contained 95% of the total area as described by Sen and Churchill (25).

For detecting epistatic interactions, the initial search for main effect QTL was followed by simultaneous search for pairs among QTL. Pairwise genome scans can detect QTL that modulate a phenotype by interacting with another quantitative trait locus, including instances in which neither locus alone reaches the significance threshold. Finally, all main effect and interacting QTL were used to fit multiple regression models. The type III sum of squares associated with each locus was used to compute the adjusted percentage of variance in the trait.

Identification of Positional QTL Candidate Genes

Using the National Center for Biotechnology Information (NCBI) online resources (http://ncbi.nlm.nih.gov), we obtained physical and gene content maps corresponding to the 95% CI for the candidate QTL. The gene content of these mouse intervals was verified by comparisons with syntenic human intervals. Gene expression (tissue origin and timing) was evaluated *in silico* using the Unigene Expressed Sequence Tag (EST) database (http://ncbi.nlm.nih.gov) and the Serial Analysis of Gene Expression (SAGE)-based Virtual Northern databases (http://cgap.nci.nih.gov). Additional computational analyses included comparison of parental strain-specific gene sequences (when available).

Validation of Predicted Strain-Specific Sequence Variations

Total kidney RNA was isolated from three 10-d-old mice from each parental strain (B6 and CAST) using TRIzol Reagent (Invitrogen, Carlsbad, CA), according to the manufacturer's recommendations, and con-

verted to cDNA using the Superscript II reverse transcriptase kit (Invitrogen). PCR amplification and sequence analyses were performed using standard methods. The B6-associated *Kif12* variant was defined by comparison with the GenBank nucleotide (BC02225) and protein (AAAH22225) *Kif12* sequences.

Gene Expression Profiling

Kidneys at the phenotypic extremes of renal disease severity were identified by averaging the severity ranks for all three renal QT. The procedures described in the GeneChip Expression Analysis Manual (Affymetrix, Inc., Santa Clara, CA) were followed to prepare cRNA targets. In brief, RNA was extracted with TRIzol, and 20 μg of RNA was used for cDNA synthesis (Superscript II Kit; Life Technologies, Rockville, MD). Biotin-labeled cRNA was generated from cDNA by *in vitro* transcription (ENZO BioArray High Yield RNA Transcript Labeling Kit; Affymetrix). Fragmented cRNA (15 μg) was hybridized to the GeneChip Mouse Genome 430 2.0 Array. The arrays were washed and stained according to the manufacturer's instructions.

The summary signal intensity for each gene was computed with *RMA* default method (27) that included *Rma* background correction, quantile normalization, and medium polish. The summary signal intensities for individual genes then were used to assess variance of the array data. These analyses included use of Fs- (28) and MAANOVA- (29) based function and adjustment of tabulated *P* values with q-value software (30,31).

Quantitative PCR

Quantitative analysis of *Kif12* expression was performed in three kidney cDNA templates from each parental strain using the LightCycler and the FastStart DNA Master SYBR Green I (Roche Diagnostics GmBH, Penzberg, Germany) according to the manufacturer's recommendations. Primers Kif12-F (5′-ACGAGGCTTCTATGTGGAACAG-3′) and Kif12-R (5′-GAGGTACCTGCTGAGAAGTTGG-3′) amplified a 184-bp product. We designed primers for three "housekeeping" reference genes: (*1*) *Actb* (encoding β-actin) Actb-F (5′-GGAGGGGCCG-GACTCATCGTACTC-3′) and Actb-R (5′-CCGCATCCTCTTCCTC-CCTGGAGAAA-3′) amplified a 416-bp product; (*2*) *Ubb* (encoding ubiquitin) Ubb-F (5′-CGGTCTTTCTGTGAGGGTGT-3′) and Ubb-R (5′-TTCACGTTCTCGATGGTGTC-3′) amplified a 159-bp product; and (*3*) *Ywhaz* (encoding tyrosine-3-monooxygenase zeta peptide) Ywhaz-F (5′-AGCAGGCAGAGCGATATGAT-3′) and Ywhaz-R (5′-GAAGCATT-GGGGATCAAGAA-3′) amplified a 288-bp product.

The amplification program consisted of initial denaturation at 95°C for 10 s, 20°C/s temperature transition ramp up to 95°C for 10 s, 60°C for 20 s. and 72°C for 30 s, repeated for 36 cycles. The threshold cycles were calculated using the LightCyler software version 3.3. To assess the significance of *Kif12* differential expression, we calculated a gene expression normalization factor for each kidney cDNA sample on the basis of the geometric mean of the housekeeping genes *Actb*, *Ubb*, and *Ywhaz* using the geNorm program (32) (http://medgen31.ugent.be/jvdesomp/genorm).

Results

Phenotypic Characterization

Of the 2031 F2 progeny generated from the (B6-*cpk*/+ × CAST/Ei)F1 intercross, 461 (23%) *cpk* mutants were identified by both phenotype and genotype criteria, a frequency consistent with the Mendelian distribution of an autosomal recessive trait. Renal disease severity was assessed by measurements of KL and KW, a standard approach used to gauge renal cystic disease severity in mice (11,13). In addition, we measured Kvol, a trait that has been recently recognized as a prognostic marker of PKD progression (33). All renal traits (KL, KW, and Kvol) varied significantly in the test cohort (Figure 1A). With KW, for example, the average weight among the 10 most minimally affected kidneys was slightly greater than normal kidneys (approximately 40 to 60 mg), whereas among the 10 most severely affected kidneys, the average weight was more than eight times higher (Table 1). All renal QT were approximately normally distributed and strongly intercorrelated (Table 2). In contrast, correlations between renal traits and CR length or BW were weak (Table 2), suggesting that additional independent QTL modulate body parameters in this cohort.

From the 461 F2 mice, 458 livers were scored by a single blinded observer. For validating the initial scoring, repeat analyses were performed on a second set of sections. Of the original 458 samples, adequate sections and consistent scores were obtained for 325 livers. Repeat scoring in the remaining 133 liver samples was confounded by insufficient tissue, suboptimal paraffin embedding, or insufficient portal triads per section. These

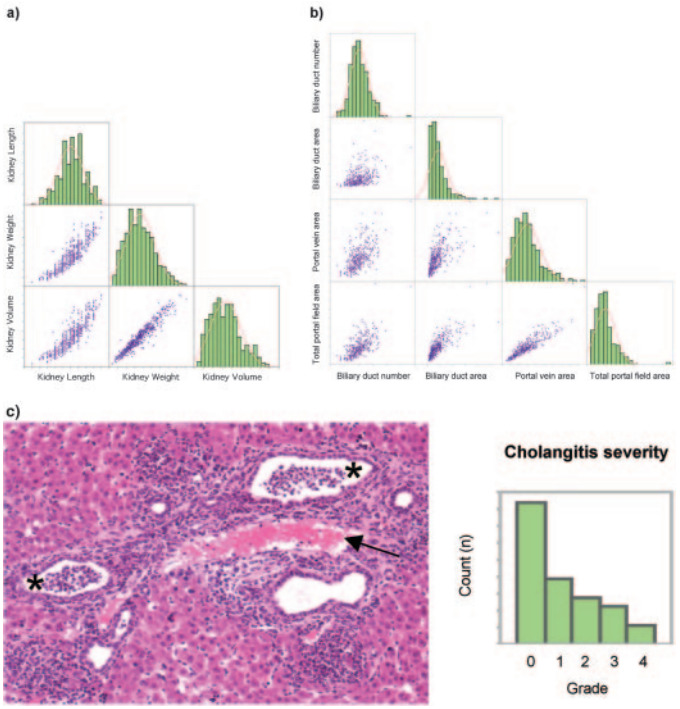

Figure 1. Quantitative traits. Histograms show the distribution of the quantitative traits (QT) for renal cystic disease (A), biliary dysgenesis (B), and cholangitis (C). Whereas the renal traits and the biliary duct number (BDN) were near-normally distributed, the distribution of the biliary duct area (BDA), portal vein area (PVA), and total portal field area (TOTA) traits were skewed to the right. (C) Grade 4 cholangitis with inflammatory cell infiltrates surrounding and filling the lumen of dilated biliary ducts (*). The arrow indicates the portal vein. The distribution of the cholangitis severity was prominently right skewed. Plots shown here and Pearson correlation coefficients shown in Table 1 demonstrate strong correlations among the renal traits; moderate correlations among BDN, BDA, and PVA; and significant correlations only between BDA and the renal traits.

Table 1. Renal phenotypic extremes and *Kif12* haplotypes[a]

Phenotype	Gender	KL (mm)	KW (g)	Kvol (ml of Water Displacement)	*Kif12* Haplotypes
Mild	F	7.0	0.09	0.09	B
Mild	F	7.0	0.08	0.09	B
Mild	M	7.0	0.09	0.08	B
Mild	F	7.5	0.08	0.09	B
Mild	F	7.0	0.08	0.09	B
Mild	M	6.0	0.04	0.03	B
Mild	F	7.3	0.11	0.12	B
Mild	M	8.3	0.12	0.12	B
Mild	F	7.5	0.10	0.10	B
Mild	M	8.0	0.09	0.11	B
Severe	M	15.0	0.91	0.75	C
Severe	F	14.0	0.76	0.71	C
Severe	F	14.0	0.78	0.68	H
Severe	M	13.0	0.57	0.49	C
Severe	M	14.0	0.64	0.52	H
Severe	M	14.0	0.78	0.58	H
Severe	F	14.0	0.73	0.67	B
Severe	M	14.3	0.72	0.74	H
Severe	F	13.0	0.67	0.64	H
Severe	M	15.0	0.85	0.78	H

[a]KL, kidney length; KW, kidney weight; Kvol, kidney volume; *Kif12* haplotypes, composed of single-nucleotide polymorphisms mCV24480597, mCV24480596, mCV24480595, mCV24480588, and mCV24480587; B, B6; H, heterozygote; C, CAST.

Table 2. Pearson correlation of quantitative traits[a]

Traits	KL	KW	Kvol	KL/CR	CR	BW	BDN	BDA	PVA	TOTA
KW	0.89[b]									
Kvol	0.88[b]	0.95[b]								
KL/CR	0.82[b]	0.76[b]	0.73[b]							
KW/BW	0.76[b]	0.86[b]	0.83[b]	0.84[b]						
CR	0.13[c]	0.12[d]	0.10[d]	−0.45[b]						
BW	0.28[b]	0.29[b]	0.26[b]	−0.22[b]	0.84[b]					
BDN	—	—	—	—	—	—				
BDA	0.15[c]	0.18[c]	0.19[c]	0.19[c]	−0.11[d]	—	0.40[b]			
PVA	—	—	—	—	—	—	0.58[b]	0.63[b]		
TOTA	—	—	—	—	—	0.12[d]	0.65[b]	0.80[b]	0.89[b]	
Cholangitis	0.10[d]	—	—	0.16[c]	−0.14[c]	−0.11[d]	—	—	—	—

[a]CR, crown-rump length; BW, body weight; BDN, bile duct number; BDA, bile duct area; PVA, portal vein area; TOTA, total portal field area.
[b]$P < 0.001$.
[c]$P < 0.01$.
[d]$P < 0.05$.

samples were excluded from phenotypic correlation studies and QTL analyses of the liver phenotypes.

We scored the components of the DPM as quantitative traits: BDN, BDA, and TOTA as a surrogate index of peribiliary fibrosis. The PVA was also assessed to provide an internal cross-sectional standard for each portal triad. BDN and BDA were normalized as the ratios BDN/PVA and BDA/PVA to adjust for potential variance in the angle of sectioning. Whereas BDN was near-normally distributed in the test cohort, the distributions of BDA, PVA, and TOTA were skewed to the right (Figure 1B). Biliary traits (BDN and BDA) and PVA were moderately intercorrelated (Table 2). Stronger correlations among BDA, PVA, and TOTA ($r = 0.80$ to 0.89) most likely reflect that BDA and PVA are major components of TOTA. The correlation of renal and biliary QT was minimal, with a significant relationship evident only for BDA ($r = 0.15$ to 0.19; $P < 0.01$). This

correlation increased to 0.31 ($P < 0.001$) when the three renal QT were converted to a single composite metric, renal PC1, and BDA was adjusted to log (BDA/PVA; see below).

Among the 458 livers evaluated, 257 (56%) had histopathologic evidence of suppurative cholangitis and/or hepatitis. Some sections contained focal collections of Gram-negative bacteria (data not shown). We defined this inflammatory lesion as a quantitative trait and determined that its distribution was right skewed (Figure 1C). There was virtually no correlation between the cholangitis QT and biliary duct dilation, as measured by BDA, or between cholangitis and the degree of periportal fibrosis assessed by TOTA (Table 2). Weak positive correlation was found between cholangitis and KL ($r = 0.10$), and a weak negative correlation was found between cholangitis and CR length ($r = -0.14$) or BW ($r = -0.11$).

Genotyping and QTL Analyses

We genotyped the affected F2 mice with 79 microsatellite markers, five of which were replaced because of segregation distortion. Using the genotypes for the final 79 markers, we computed a genetic map with Pseudomarker software version 1.02 and confirmed the designated marker order in our intercross.

As the renal QT (KL, KW, and Kvol) were strongly intercorrelated, we converted these individual traits to a single composite metric (renal PC1) using principal component analysis (34). In addition, logarithmic and square root transformations were applied to traits with skewed distributions (*e.g.*, BDA, PVA, TOTA; Figure 1B) to normalize their distributions and optimize subsequent QTL analyses. The statistical power of these analyses was further enhanced by the logarithmic transformation of the BDA to PVA ratio (log[BDA/PVA]), an index of biliary ductal expansion.

Genome-wide scans with Pseudomarker 1.02 identified a significant main effect QTL on Chr 4 that was common for the composite renal trait (renal PC1), biliary ductal expansion (expressed as log[BPA/PVA]), and cholangitis (Figure 2). The broad QTL peak and high logarithm of odds (LOD) score suggest that the Chr 4 interval may harbor multiple loci affecting these traits. Additional significant QTL mapped to Chr 1 and 2 for renal PC1 and Chr 13 for biliary ductal expansion (log[BDA/PVA]; Figure 2).

The Chr 4 main effect was fitted with models that comprised one, two, and three QTL; maximum LOD scores were calculated for each; and permutation testing was used to determine significance thresholds. These analyses suggest the presence of at least three QTL intervals on Chr 4 that contribute to renal PC1 (Table 3, Figure 3A). Both double-QTL and triple-QTL models had similar significance levels with maximal LOD scores 21 to 22. Such high LOD scores allowed "conditioning" on individual QTL peaks to determine their impact on the complex main effect. On the basis of these analyses, we excluded the putative QTL at 42 and 26 cM as a false or "ghost" QTL and refined the Chr 4 main effect to a three-QTL complex extending from 10 to 58 cM (95% CI) with QTL peaks at 16, 34, and 54 cM (Table 3).

All main effect renal QTL (Figure 3B) and their interactions were tested in multiple regression models. Whereas CAST alleles at the Chr 4 QTL exerted dominant effects, CAST alleles at the Chr 1 and Chr 2 loci had additive effects on disease severity (Table 3, Figure 3B).

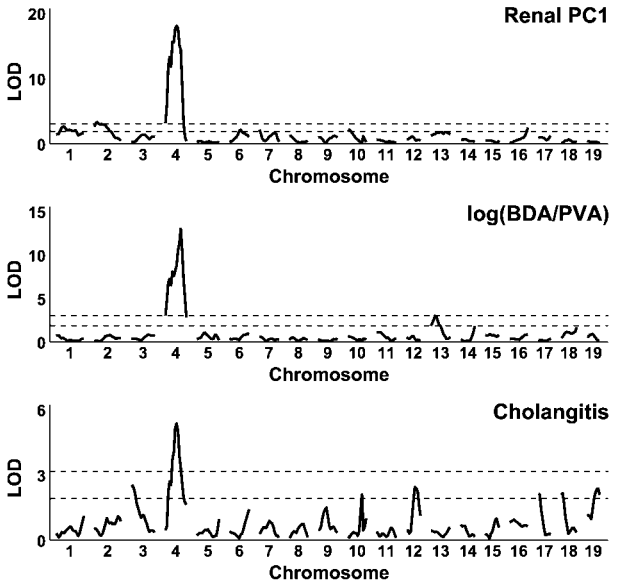

Figure 2. A major-effect quantitative trait loci (QTL) complex on chromosome (Chr) 4. Whole-genome scans identified a major-effect QTL complex on Chr 4 that modulates the three traits: Renal principal component 1 (PC1; see text), biliary ductal expansion, and cholangitis. Renal PC1 incorporated all three renal traits (kidney length [KL], kidney weight [KW], and kidney volume [Kvol]); biliary ductal expansion represented the logarithmic transformation of the BDA to PVA ratio log(BDA/PVA). The upper and lower horizontal lines in each scan represent significant ($P = 0.05$) and suggestive ($P = 0.1$) logarithm of odds (LOD) thresholds, respectively, as determined by permutation testing among 1000 permutations.

Initial QTL analyses identified a main effect for biliary duct expansion log(BDA/PVA) on Chr 4 (Figure 4A). In addition to the Chr 4 QTL, multiple regression modeling confirmed a significant QTL on Chr 13 (Table 3, Figure 4B), as well as two sets of interactions between Chr 1 at 62 cM and Chr 2 at 96 cM and Chr 4 at 14 cM and Chr 18 at 17 cM (Figure 4C). Gender was used as an additive covariate. This model explained approximately 37% of the phenotypic variability. Although the multiple regression model for cholangitis included the Chr 4 QTL and two additional significant QTL on Chr 3 and 19 (Figure 4, D and E), no significant QTL interactions were observed. Gender again was used as an additive covariate. This model explained approximately 10% of the observed variability. All of the individual, non–Chr 4 QTL were phenotype specific. The chromosomal positions of these QTL and their dominance characteristics are summarized in Table 3.

Identification and Characterization of Positional Candidate Genes for the Renal QT

Among the strategies to identify genes that underlie major QTL effects, refined interval mapping using congenic strains is

Table 3. Main-effect QTL[a]

Traits	Chr	Location (cM)	95% CI	Max LOD	% Variance	CAST Effect
Renal PC1	1	26	10 to 39	2.5	2.1	A
	2	8	0 to 18	3.2	1.8	A
	4a	16	10 to 58	5.0	2.2	D
	4b	34	10 to 58	7.0	2.1	D
	4c	54	10 to 58	6.0	5.2	D
Biliary ductal expansion	4a	14	0 to 58	1.8	2	D
	4b	34	0 to 58	1.2	1.4	D
	4c	52	0 to 58	5.8	6.8	D
	13	16	2 to 32	6.8	6.5	OD
Cholangitis	3	6	0 to 30	3.3	3.1	A
	4	34	32 to 50	4.8	4.5	OD
	19	40	8 to 48	2.7	2.5	A

[a]QTL, quantitative trait loci; Chr, chromosome; LOD, logarithm of odds; CI, confidence interval; A, additive; D, dominant, R, recessive; OD, overdominant.

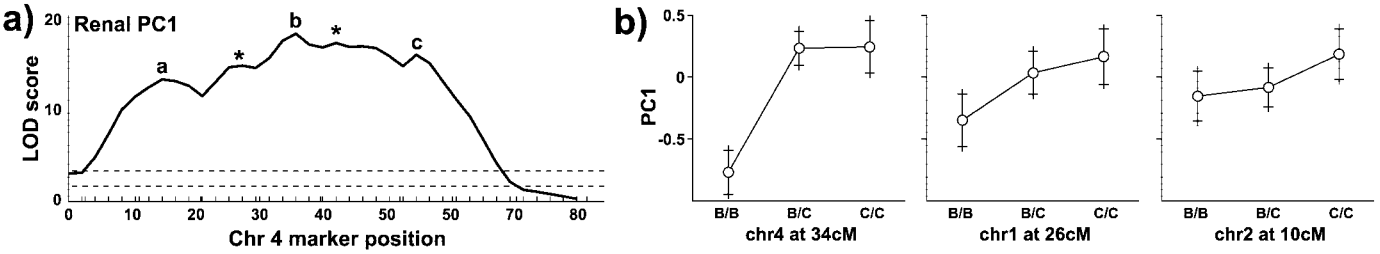

Figure 3. Main-effect QTL and an interaction model for renal disease severity. (A) Chr 4 major-effect QTL complex. "Conditioning" on the individual QTL peaks revealed that the Chr 4 QTL consists of a triple-QTL complex instead of the five-peak QTL observed in the initial analysis. The true Chr 4 peaks map to 16 (A), 34 (B), and 54 cM (C; see also Table 1); the false or "ghost" peaks at 26 and 42 cM are designated by "*." (B) All main effect loci and mean value for allelic combinations at each locus. BB denotes homozygosity for B6 alleles, and CC denotes homozygosity for CAST alleles. Approximate 95% confidence intervals (CI; mean ± 2 SEM) are shown for each allelic combination. The Chr 4 QTL exerted a dominant CAST effect, whereas the CAST allele at the Chr 1 and Chr 2 loci had an additive effect on severity.

the most standard but also the most time and labor intensive. Therefore, we developed a set of alternative strategies using gene-expression profiling, computational analyses, and SNP-based haplotyping to prioritize the positional candidate genes for the renal QTL. Similar strategies have led to the successful identification of QTL candidate genes in other systems (35–37).

Our search for candidate genes focused on the 10- to 58-cM interval on Chr 4. This interval corresponds to 24 to 124 Mbp on the physical map and contains approximately 800 genes (http://ncbi.nlm.nih.gov). Virtually all of these genes are represented on the GeneChip Mouse Genome 430 2.0 Array. We examined the gene expression profiles in kidneys from 10-d-old mice representing the phenotypic extremes within the F2 cohort (seven kidneys from each phenotypic tail). We detected approximately 2500 genes that were differentially expressed at $P \leq 0.0005$. Greater than twofold change in expression was observed in 374 genes, among which 23 genes mapped to the Chr 4 candidate QTL interval (Table 4). Using computational analyses, we determined that seven of these 23 genes are expressed in both kidney and liver, organs that express the major *cpk* phenotypes (Table 4).

To prioritize the analysis of positional candidate QTL genes, Wang *et al.* (37) evaluated the SNP-based haplotypes for each candidate gene and excluded those with identical parental strain haplotypes, because these genes originated in a common mouse ancestor. We therefore examined the SNP-based haplotypes for our seven positional candidate genes. B6 and CAST-specific haplotypes were identified for two genes, *Kif12* (encoding kinesin family member 12) and *Ptprd* (encoding protein tyrosine phosphatase, receptor D), whereas the parental haplotypes were identical in the remaining five genes. We identified allele-specific sequence variants for both the *Kif12* and *Ptprd* transcripts. However, whereas the variation in *Ptprd* involved a relatively conservative tyrosine to phenylalanine transition (38), the *Kif12* variant involves a 15-bp deletion in the B6 allele (c.217_231del15) that corresponds to a five–amino acid deletion (p.61_65del5) in the predicted L2 loop of the catalytic domain of the kinesin molecular motor (Figure 5).

Kif12 *Is a Candidate* cpk *Modifier Gene*

Additional analyses further supported *Kif12* as a strong QTL candidate gene. We examined the *Kif12* haplotype in the 10

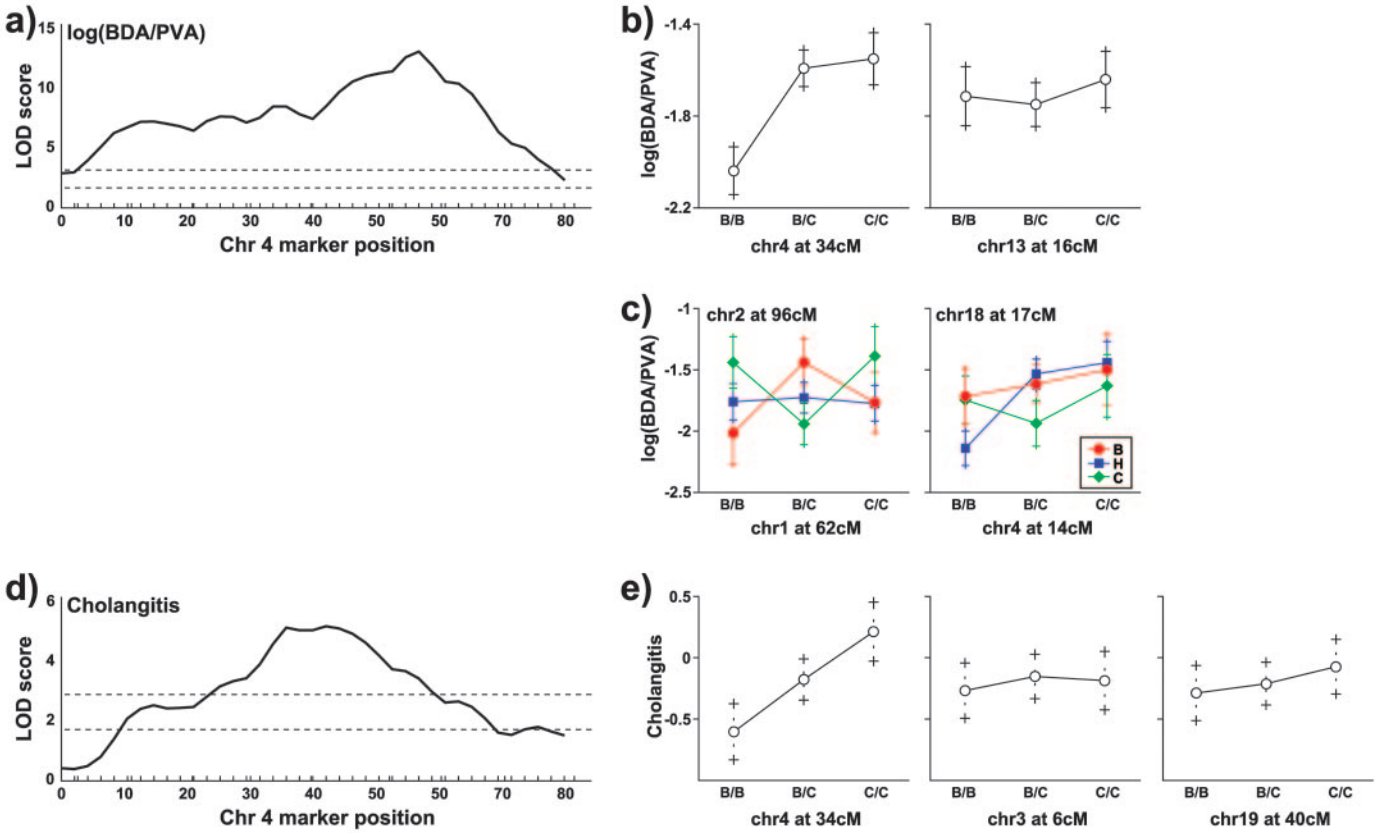

Figure 4. Main-effect QTL and pairwise interactions for biliary traits and cholangitis. The Ch 4 QTL complex also exerted a major effect on biliary ductal expansion (A) and cholangitis (D). Main effects and pairwise interactions are shown for the biliary trait (B and C) and cholangitis (E). The mean value of each trait for allelic combinations of one or two loci is indicated. BB denotes homozygosity for B6 alleles, and CC denotes homozygosity for CAST alleles. Approximate 95% CI (mean ± 2 SEM) are shown. For biliary ductal expansion, a dominant CAST effect was observed for the Chr 4 QTL, whereas the CAST effect was overdominant for the Chr 13 locus. Two pairwise interactions were identified for biliary trait severity. The Chr 1 and Chr 2 loci show a complex pattern of interaction in that the effect of the Chr 1 locus on log(BDA/PVA) is absent when the Chr 2 locus is heterozygous but displays opposing overdominant (heterotic) patterns when the Chr 2 locus is homozygous for BB or CC. The effect of the Chr 4 QTL seemed to be enhanced and more distinctly dominant when there was at least one B6 allele at the Chr 18 locus. For cholangitis severity, the CAST allele at the Chr 3 and Chr 19 QTL had additive effects, whereas the CAST effect was overdominant for the Chr 4 locus.

most severely *versus* 10 least severely affected F2 *cpk* mice and determined that the CAST haplotype was strongly associated with disease severity (χ^2 16.36, $P < 0.001$). Consistent with the dominant CAST effect on renal disease severity, 90% of the severely affected mice had at least one CAST-derived *Kif12* haplotype, whereas 100% of the mildly affected mice were homozygous for the B6 haplotype (Table 1).

When normalized for the reference "housekeeping genes" *Ubb* and *Ywhaz*, *Kif12* expression was significantly different ($P = 0.016$) in kidneys from 10-d-old wild-type B6 mice when compared with age-matched wild-type CAST mice (Figure 6). These data suggest that the differences observed with respect to *Kif12* expression in F2 *cpk* kidneys likely reflects differences in parental strain-specific expression, rather than a secondary change related to *cpk*-related disease severity.

Furthermore, analysis of the NCBI EST database reveals that 50% of the *Kif12*-related EST are expressed in neonatal mouse kidney, with an additional 29% of the EST derived from kidneys of unspecified age. The remaining *Kif12* EST derive from four other tissues, including liver and pancreas, organs that express the major *cpk* phenotypes (22). SAGE-based analysis of the human nephron segments (GEO ID: GDS503) (39) demonstrates that *KIF12* is predominantly expressed in collecting ducts, the principal nephron segment that undergoes cystic change in the *cpk* mouse.

Discussion

QTL that exert main effects on renal cystic disease have been reported for several murine PKD models (reviewed in 10). In contrast to the extensive search for renal QTL, limited effort has been directed toward identifying loci that modulate the progression of CHF, a major ARPKD-associated phenotype and significant cause of morbidity and mortality in older children (24).

The current study represents the first quantitative analyses of both the renal and biliary phenotypes expressed in the *cpk*

Table 4. Differential expression in Chr 4 positional QTL candidate genes

#	Probe ID	Over-Expressing Phenotype	N-fold Increased Expression	P Value	GenBank#	Gene Symbol	Description	NCBI ESTs Total	Kidney ESTs [%]	Liver ESTs [%]	Map	Chr 4 QTL Peak	Kidney ESTs	Liver ESTs
1	1450771	mild	2.3	0.001123999	NM_010243	Fut9	fucosyltransferase 9	79	27	0	chr4:25818239-25818812 (+)	16 cM	21	0
1	1457409	mild	2.2	0.001086276	BB484070	Fut9	fucosyltransferase 9	79	27	0	chr4:25822652-25823075 (+)	16 cM	21	0
2	1435308	mild	2.5	0.001086276	AU067636	—	Mus musculus adult female vagina cDNA	37	35	0	chr4:25827189-25827638 (+)	16 cM	13	0
3	**1425150**	**severe**	**2.7**	**0.0015318**	**BC010829**	**C730036D15Rik**	**RIKEN cDNA C730036D15 gene**	**29**	**52**	**31**	**chr4:49023779-49024167 (−)**	**34 cM**	**15**	**9**
4	**1453193**	**mild**	**2.3**	**0.001141442**	**AK018598**	**Kif12**	**kinesin family member 12**	**42**	**79**	**2**	**chr4:61730529-61731682 (−)**	**34 cM**	**33**	**1**
5	1432591	severe	2.8	0.001086276	BB635017	—	Mus musculus 0 day neonate head cDNA	9	0	0	chr4:63921632-63922133 (+)	34 cM	0	0
6	1429052	mild	2.2	0.001073569	AK003303	—	Mus musculus 12 days embryo head cDNA	52	4	0	chr4:74394044-74394565 (−)	34 cM	2	0
7	**1424886**	**mild**	**2.8**	**0.001073569**	**BC025145**	**Ptprd**	**protein tyrosine phosphatase, receptor D**	**112**	**14**	**3**	**chr4:74397622-74406923 (−)**	**34 cM**	**16**	**3**
8	1443056	mild	2.2	0.001073569	BB374993	—	Mus musculus 16 days embryo head cDNA	5	0	0	chr4:74654255-74654694 (−)	34 cM	0	0
9	1441498	mild	2.5	0.001086276	AW546318	—	Mus musculus transcribed sequences	13	0	0	chr4:74770555-74770941 (−)	34 cM	0	0
10	1440624	mild	4	0.001073569	BB477150	—	Mus musculus transcribed sequences	—	—	—	chr4:74771233-74771778 (−)	34 cM	—	—
11	1442837	mild	4.3	0.001066266	BB134628	—	Mus musculus adult male bone cDNA	4	0	0	chr4:74840328-74840812 (−)	34 cM	0	0
12	1444622	mild	2.1	0.001073569	BM118846	—	Mus musculus 16 days neonate thymus cDNA	5	40	0	chr4:74851048-74851463 (−)	34 cM	2	0
13	1443053	mild	3.7	0.001086276	BB523104	—	Mus musculus 15 days embryo head cDNA	5	0	0	chr4:74888287-74888702 (−)	34 cM	0	0
14	1443075	mild	2.7	0.001086276	AW556334	—	Mus musculus transcribed sequences	—	—	—	chr4:74894293-74894788 (−)	34 cM	—	—
15	1429488	mild	2.1	0.001201747	AK017682	Zdhhc21	zinc finger, DHHC domain containing 21	83	2	0	chr4:81405230-81405727 (−)	54 cM	2	0
16	1439852	mild	2.2	0.001157847	BB036443	—	Mus musculus transcribed sequences	—	—	—	chr4:82940006-82940550 (−)	54 cM	—	—
17	1453345	severe	2.1	0.001073569	AK014427	3830408G10Rik	RIKEN cDNA 3830408G10 gene	79	0	14	chr4:90819741-90820162 (−)	54 cM	0	11
18	**1417531**	**mild**	**2.2**	**0.001095959**	**BF783609**	**Cyp2j5**	**cytochrome P450, family 2, subfamily j5**	**195**	**68**	**15**	**chr4:95677584-95677956 (−)**	**54 cM**	**133**	**29**
19	**1421830**	**mild**	**2.4**	**0.001528605**	**NM_009647**	**Ak4**	**adenylate kinase 4**	**240**	**6**	**1**	**chr4:100326137-100326387 (+)**	**54 cM**	**15**	**3**
20	1433596	mild	2.4	0.001073569	BQ175337	Dnajc6	DnaJ (Hsp40) homolog, subfamily C6	179	2	0	chr4:100501957-100502430 (+)	54 cM	3	0
21	1427308	severe	2.4	0.001086276	BB644109	C630028C02Rik	RIKEN cDNA C630028C02 gene	58	5	0	chr4:103602026-103602403 (+)	54 cM	3	0
22	**1417991**	**mild**	**2.3**	**0.001115732**	**NM_007860**	**Dio1**	**deiodinase, iodothyronine, type I**	**45**	**22**	**40**	**chr4:106151238-106151765 (−)**	**54 cM**	**10**	**18**
23	**1417462**	**severe**	**2.6**	**0.001528427**	**NM_007598**	**Cap1**	**CAP, adenylate cyclase-associated protein 1**	**526**	**2**	**2**	**chr4:121924877-121927503 (+)**	**54 cM**	**13**	**11**
23	**1417461**	**severe**	**2.3**	**0.001743061**	**NM_007598**	**Cap1**	**CAP, adenylate cyclase-associated protein 1**	**526**	**2**	**2**	**chr4:121927936-121928323 (+)**	**54 cM**	**13**	**11**

bold font indicates expression in both kidney and liver.

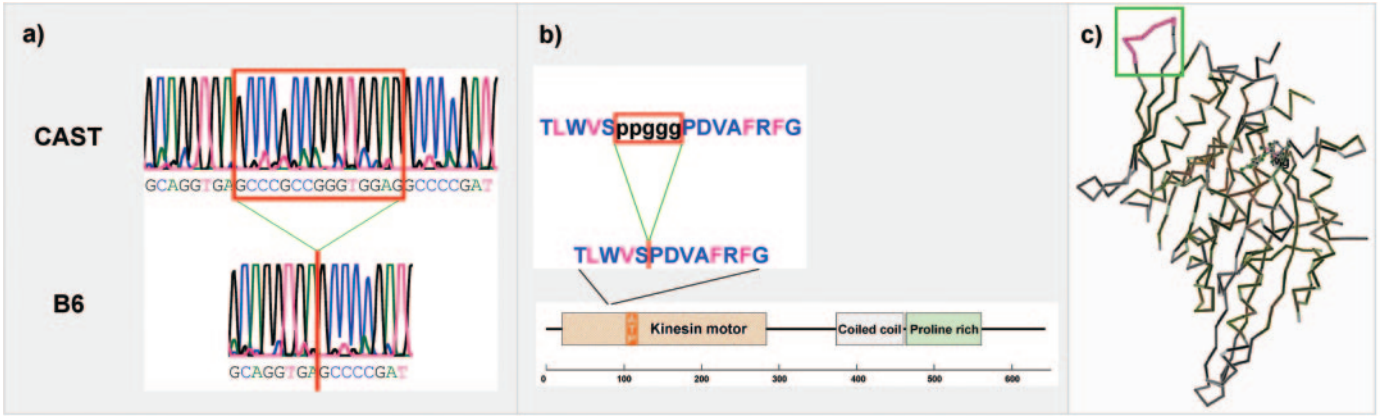

Figure 5. Kif12 allelic variants. Sequence analysis of B6 and CAST transcripts revealed a 15-bp deletion variant (A) that corresponds to 5–amino acid deletion in the kinesin motor domain (red box; B). In the three-dimensional model of the related kinesin motor domain encoded by yeast *kar3*, the predicted deletion involves the L2 loop, indicated by a red line (C).

model of ARPKD. Several lines of evidence indicate that genetic background modulates both *cpk* phenotypes. In a preliminary study, Woo *et al.* (11) demonstrated that progression of renal cystic disease in *cpk* mice is a quantitative trait under polygenic control. Whereas B6-*cpk/cpk* mice do not express a biliary lesion (16), our group and others have shown that the phenotype is fully penetrant in *cpk* mutants derived from experimental crosses and congenic strains (19,22). These observations suggest that whereas genetic background modulates the expression of both the renal cystic and the biliary traits, at least some of the *cpk* modifier genes exert an organ-specific effect (19).

In the F2 cohort that we generated from a (B6-+/*cpk*× CAST)F1 intercross, we defined the renal cystic disease as three quantitative traits based on KL, KW, and Kvol. KL is a common parameter used in pediatric renal imaging, and Kvol measured by magnetic resonance imaging has emerged as a prognostic marker of PKD progression (33). In our test cohort, we used a water displacement technique to measure Kvol *ex vivo*. The validity of this metric is supported by its strong correlation with the other renal QT.

Previous studies have used the ratios KL/CR and KW/BW to adjust for runting in severely affected mice. Therefore, we performed QTL analyses with these ratios as well as KL, KW, and Kvol. Although similar main-effect QTL were identified for all of these traits (data not shown), we note that multiple QTL have main effects on body size alone, *e.g.*, BW (41). We therefore expect that these loci may modulate CR and BW independent of PKD severity, and we excluded these ratios from further anal-

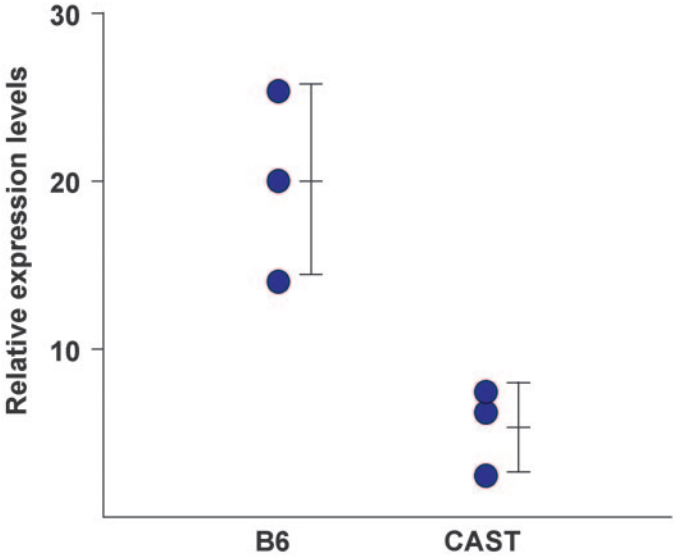

Figure 6. Differential *Kif12* expression levels in kidneys from the B6 and CAST parental strains. For each strain, $n = 3$ kidneys; bars indicates mean ± 1 SD. Quantitative PCR data were normalized with geNorm program using geometric means of two housekeeping genes, *Ubb* and *Ywhaz*.

yses. Because the single renal traits were strongly intercorrelated, we converted these individual QT to a single composite metric, renal PC1 (34). The combination of correlated variables into one robust factor allows a reduction of dimension without significant data loss. In fact, our data are consistent with previous reports that demonstrate 30 to 100% improvement in statistical power when QTL analyses are performed on composite traits *versus* single traits (34).

In addition, we quantified the biliary (BDN and BDA), venous (PVA), and matricellular components (TOTA) of the DPM that underlies CHF. Whereas moderate intercorrelation was found among the biliary QT, only BDA had significant correlation with the renal QT. Given that BDA provides an index of the differentiation defect in the developing biliary tree, these data may indicate a correlation between ductal epithelial defects in the kidney and the liver. That other components of the DPM lesion are not correlated with the renal QT may suggest that additional, organ-specific factors modulate CHF expression.

The histopathologic hallmark of CHF involves "chaotic" branching and dilation of the bile ductules, as well as matricellular expansion of the portal triad. We speculated that the severity of biliary lesion could be estimated best from the sum of all BDA per portal field cross-section. Similarly, we expected the severity of the associated fibrosis to be directly proportional to the total portal triad area (TOTA). We found, however, that the unadjusted BDA and TOTA had limited power in QTL analyses. This observation is perhaps not unexpected when one considers that our analyses were performed in tissue sections. Given the extensive arborization of the biliary tree, quantitative assessment of two-dimensional areas may be confounded by variability in the sectioning angle for different portal triads. In CHF, this issue is further compounded by the chaotic branching associated with the DPM. We therefore reasoned that the cross-sectional angle effect could be minimized by the use of the ratios BDA/PVA and BDA/TOTA and that the distribution of these traits could be optimized by logarithmic transformation. In our QTL analyses, log(BDA/PVA) proved to be much more robust than log(BDA/TOTA). On the basis of our findings, we propose that future quantitative analyses of the DPM lesion, in both murine models and human ARPKD, should use magnetic resonance imaging or microcomputed tomography (42) to more precisely define the three-dimensional defect in the biliary tree architecture.

A majority of the livers examined had evidence for cholangitis, prompting us to define this inflammatory lesion as a quantitative trait. We found weak correlation between cholangitis and the renal QT (KL), but there was no correlation with individual biliary QT. These data are surprising given that severe dilation of intrahepatic bile ducts (Caroli's disease) is associated with an increased risk for cholangitis in human ARPKD (43), an observation interpreted to mean that defects in biliary epithelial differentiation predispose to ascending cholangitis. Our data may suggest an alternative paradigm in which there is interplay between the primary epithelial defects and the risk for ascending cholangitis. In this model, cholangitis *per se* may exacerbate the baseline biliary ductal defect. As supportive data, we note several instances in which ARPKD infants develop dilation of intrahepatic bile ducts *de novo* after episodes of ascending cholangitis (L.M.G.-W., unpublished data).

Genome-wide scans identified a significant main-effect QTL on Chr 4 that was common for renal PC1, log(BPA/PVA), and cholangitis. It is interesting that the other significant QTL seemed to have phenotype-specific main effects, consistent with previous data suggesting organ-specific modulation for at least some of the *cpk* modifier genes (19).

We found that the Chr 4 main effect on renal PC1 involved at least three QTL. When two tightly linked loci modulate the same phenotypic trait, QTL analysis can identify a "ghost" QTL peak that is a statistical artifact positioned between the true effects of the two underlying QTL (44). To refine the Chr 4 QTL intervals and identify potential ghost QTL, we removed individual QTL peaks from our analytic model and determined the impact on the renal PC1 main effect. We used both multiple QTL modeling and conditional analysis, in which the position of one or more QTL is fixed and the region is scanned for additional QTL, to explore the number and locations of multiple effects in the Chr 4 region. The putative QTL at 26 and 42 cM were excluded as ghost QTL, and the Chr 4 main effect was refined to QTL peaks at 16, 34, and 54 cM. There was insufficient statistical power to perform similar analyses for the traits log(BPA/PVA) and cholangitis.

We note that PKD severity in the *jck* (14) and *pcy* (12) models is also modulated by proximal Chr 4 QTL. It is difficult to compare our analyses with these data because of the differences in genetic background and experimental crosses. However, both the current study and the previous reports identify a broad QTL peak centered on approximately 25 cM. Given the

statistical power of our analyses, we were able to perform appropriate conditioning and exclude this peak as a ghost QTL. It therefore is conceivable that the Chr 4 QTL reported previously are distinct from the QTL found to modulate renal PC1 in this study. Alternatively, the single reported QTL may represent the effect of two adjacent QTL, perhaps one more proximal, corresponding to the QTL at 16 cM, and one more distal, representing the main effect at 34 cM. Further studies that control for genetic background and ghost QTL will be required to resolve this issue.

QTL intervals are broad, and defining a set of plausible candidate genes typically involves construction of recombinant consomic/congenic strains and bioinformatics approaches to refine the QTL interval. Ultimately, a transgenic or knockout/knock-in strategy is required to validate the candidate gene (45).

Alternative approaches for identifying genes that underlie QTL main effects recently have allowed effective prioritization among positional candidates and the subsequent identification of QTL genes. One approach that prioritized candidate genes on the basis of differential expression in mildly and severely affected individuals has successfully identified *CD36* as insulin resistance QTL1 (35) and *C5* as a susceptibility locus for asthma (36). Therefore, we used gene expression profiling to determine positional candidate genes that were differentially expressed in *cpk* mice with mild *versus* severe cystic kidney disease. We then determined which of these candidates was expressed in kidney and liver, organs involved in the traits associated with Chr 4 QTL, and excluded QTL candidate genes with identical parental haplotype blocks, reflecting derivation from a common recent ancestor (37).

To complement these strategies we then comprehensively evaluated the expression and sequence variants of positional candidate genes using computational analyses through NCBI, *e.g.*, UniGene, Virtual Northern, and LocusLink. Specifically, we examined all positional QTL candidates and identified genes with expression in expected target tissue(s), including appropriate temporal expression and protein localization. Then, we further prioritized selected candidates on the basis of biologic function and differential expression. Finally, we examined available information regarding variation in coding or regulatory sequences and putative alternative splicing. Using this approach, we have identified *Kif12*, which encodes the kinesin family member 12, as a prime candidate gene for the Chr 4 QTL effect.

Kif12 fulfills the major criteria for QTL gene discovery established by the Complex Trait Consortium (45). Specifically, we have (*1*) identified a major QTL on Chr 4; (*2*) refined this Chr 4 main effect to QTL peaks at 16, 34, and 54 cM; (*3*) determined that *Kif12* maps beneath the QTL peak at 34 cM; (*4*) demonstrated that *Kif12* strain-specific haplotypes and *Kif12* expression levels significantly correlate with renal disease severity in our F2 intercross; (*5*) confirmed corresponding strain-specific *Kif12* expression levels in wild-type parental strains; and (*6*) identified functionally relevant sequence variants among *Kif12* transcripts derived from the B6 and CAST parental strains. As would be predicted for a *cpk* modifier gene, *Kif12* is expressed primarily in kidney, as well as in liver and pancreas. Within the kidney, *Kif12* is predominantly expressed in collecting ducts, the principal segment from which cysts arise in *cpk* kidneys.

Kif12 encodes a recently described kinesin that has yet to be assigned to a specific kinesin family (http://www.proweb.org/kinesin/). However, in the *Kif12*-encoded protein, the molecular motor is located in the N-terminus, thus putatively assigning this protein to the KinN family group that translocates cargo toward the plus end of microtubuli (46). Whereas the functional effect of a 5–amino acid (AA) deletion within the L2 loop of this family of proteins is not known, deletions in the L2 loop of a KinI kinesin diminished its microtubule depolymerization activity (47). Therefore, we speculate that the 5-AA deletion in the L2 loop of the kinesin family member 12 may modulate its interaction with microtubules. Given that microtubule instability and degradation is a critical feature underlying disease progression in the *cpk* mouse (48), the B6 allele may attenuate disease progression through functions similar to those of taxanes, drugs that markedly retard disease progression in the *cpk* mouse by promoting microtubule polymerization and stabilization (49).

Two additional lines of evidence support our assertion that *Kif12* is a candidate *cpk* modifier gene (modifier of *cpk*, *Mocpk*). First, yeast two-hybrid data indicate that the protein encoded by *Kif1a*, one of the closest protein relatives of *Kif12* (50), interacts with the *Cys1*^{cpk} gene product cystin (L.M.G.-W., submitted). Second, a renal-specific knockout of a second kinesin family gene, *Kif3a*, causes PKD (51). For further validating *Kif12* as a *Mocpk* candidate, studies to assess the intracellular distribution of kinesin family member 12 and to determine whether it interacts directly with cystin are in progress. In addition, we are generating transgenic mice that express the CAST allele of *Kif12* and will evaluate the transgene effect on disease severity in B6-*cpk*/*cpk* mice.

Finally, we note that the *Invs* gene is a strong candidate for the most proximal Chr 4 QTL at 16 cM. Mutations in *Invs* cause the *inv* phenotype, a PKD-related disorder in mice, and nephronophthisis type 2 (NPHP2) in human infants (52). Alternative splice variants encode several isoforms of the protein product inversin, and these localize to different subcellular compartments, including the nucleus and cell–cell adhesion sites (53), as well as the primary apical cilium (54). However, although both cystin and inversin localize to the primary apical cilia, it is not clear which *Invs* transcripts encode the cilia-targeted isoforms, and, thus, it is impractical to determine whether the B6 and CAST parental strains harbor functionally relevant sequence variants. Further studies are in progress (CL Phillips, Indiana University, IN, personal communication, October 2004).

In summary, this is the first study to define ARPKD-like phenotypes in an experimental model as quantitative traits. A major effect QTL complex on Chr 4 modulates the renal cystic disease and components of the biliary lesion, as well as cholangitis. Multiple regression models identify additional phenotype-specific QTL and several pairwise interactions. These additional QTL may identify organ-specific genetic pathways that are important in the pathogenesis of disease phenotypes. Ex-

pression and sequence analyses indicate that variations in *Kif12*, the gene encoding a novel kinesin, underlie the Chr 4 main effect on all three major phenotypes. Therefore, we propose that *Kif12* is a *cpk* modifier gene (*Mocpk*) and as such is the first candidate gene identified for a PKD QTL.

Acknowledgments

This work was supported by a Polycystic Kidney Disease Foundation Fellowship Award (M.M.), a Clinical Scientist Award in Translational Research from the Burroughs-Wellcome Foundation (L.M.G.-W.), and the National Institutes of Health (G.A.C.).

We thank Gbolakan Folayan for technical support and Sylvie Mrug for assistance with data analysis.

References

1. Gabow P: Autosomal dominant polycystic kidney disease. *N Engl J Med* 329: 332–342, 1993
2. The European Polycystic Kidney Disease Consortium: The polycystic kidney disease 1 gene encodes a 14 kb transcript and lies within a duplicated region on chromosome 16. *Cell* 77: 881–894, 1994
3. The American PKD1 Consortium: Analysis of the genomic sequence for the autosomal dominant polycystic kidney disease (PKD1) gene predicts the presence of a leucine-rich repeat. *Hum Mol Genet* 4: 575–582, 1995
4. The International Polycystic Kidney Disease Consortium: Polycystic kidney disease: The complete structure of the PKD1 gene and its protein. *Cell* 8: 289–298, 1995
5. Mochizuki T, Wu G, Hayashi T, Xenophontos S, Veldhuisen B, Saris J, Renolds D, Cai Y, Gabow P, Pierides A, Kimberling WJ, Breuning MH, Deltas CC, Peters DJ, Somlo S: PKD2, a gene for polycystic kidney disease that encodes an integral membrane protein. *Science* 272: 1339–1342, 1996
6. Onuchic L, Furu L, Nagasawa Y, Hou X, Eggermann T, Ren Z, Bergmann C, Senderek J, Esquivel E, Zeltner R, Rudnik-Schoneborn S, Mrug M, Sweeney W, Avner ED, Zerres K, Guay-Woodford LM, Somlo S, Germino GG: *PKHD1*, the polycystic kidney and hepatic disease 1 gene, encodes a novel large protein containing multiple IPT domains and PbH1 repeats. *Am J Hum Genet* 70: 1305–1317, 2002
7. Ward C, Hogan M, Rossetti S, Walker D, Sneddon T, Wang X, Kubly V, Cunningham J, Bacallao R, Ishibashi M, Milliner DS, Torres VE, Harris PC: The gene mutated in autosomal recessive polycystic kidney disease encodes a large, receptor-like protein. *Nat Genet* 30: 259–269, 2002
8. Hateboer N, Lazarou L, Williams A, Holmans P, Ravine D: Familial phenotype differences in PKD1. *Kidney Int* 56: 34–40, 1999
9. Guay-Woodford LM, Desmond RA: Autosomal recessive polycystic kidney disease: The clinical experience in North America. *Pediatrics* 111: 1072–1080, 2003
10. Guay-Woodford L: Murine models of polycystic kidney disease: Molecular and therapeutic insights. *Am J Physiol Renal Physiol* 285: F1034–F1049, 2003
11. Woo D, Miao S, Tran T: Progression of polycystic kidney disease in cpk mice is a quantitative trait under polygenic control [Abstract]. *J Am Soc Nephrol* 6: 731A, 1995
12. Woo D, Nguyen D, Khatibi N, Olsen P: Genetic identification of two major modifier loci of polycystic kidney disease progression in *pcy* mice. *J Clin Invest* 100: 1934–1940, 1997
13. Guay-Woodford L, Walz G, Wright C, Churchill G: Quantitative trait loci (QTLs) that influence renal cystic disease severity in the mouse bpk model. *J Am Soc Nephrol* 11: 1253–1260, 2000
14. Kuida S, Beier D: Genetic localization of interacting modifiers affecting severity in a murine model of polycystic kidney disease. *Genome Res* 10: 49–54, 2000
15. Preminger G, Koch W, Fried F, McFarland E, Murphy E, Mandell J: Murine congenital polycystic kidney disease: A model for studying development of cystic disease. *J Urol* 127: 556–560, 1982
16. Fry J, Koch W, Jennette J, McFarland E, Fried F, Mandell J: A genetically determined murine model of infantile polycystic kidney disease. *J Urol* 134: 828–833, 1985
17. Hou X, Mrug M, Yoder B, Lefkowitz E, Kremmidiotis G, D'Eustachio P, Beier D, Guay-Woodford L: Cystin, a novel cilia-associated protein, is disrupted in the *cpk* mouse model of polycystic kidney disease. *J Clin Invest* 109: 533–540, 2002
18. Yoder B, Hou X, Guay-Woodford L: The polycystic kidney disease proteins, polycystin-1, polycystin-2, polaris, and cystin, are co-localized in renal cilia. *J Am Soc Nephrol* 13: 2508–2516, 2002
19. Guay-Woodford L, Green W, Lindsey J, Beier D: Germline and somatic loss of function of the mouse *cpk* gene causes biliary ductal pathology that is genetically modulated. *Hum Mol Genet* 9: 769–778, 2000
20. Avner E, Studnicki F, Young M, Sweeney W, Piesco W, Ellis D, Fetterman G: Congenital murine polycystic kidney disease. I. The ontogeny of tubular cyst formation. *Pediatr Nephrol* 2: 210–218, 1987
21. Gattone V, Ricker J, Trambaugh C, Klein R: Multiorgan mRNA misexpression in murine autosomal recessive polycystic kidney disease. *Kidney Int* 62: 1560–1569, 2002
22. Ricker J, Gattone V, Calvet J, Rankin C: Development of autosomal recessive polycystic kidney disease in BALB/c-*cpk/cpk* mice. *J Am Soc Nephrol* 11: 1837–1847, 2000
23. Gattone V, MacNaughton K, Kraybill A: Murine autosomal recessive polycystic kidney disease with multiorgan involvement induced by the cpk gene. *Anat Rec* 245: 488–499, 1996
24. Guay-Woodford L, Jafri Z, Bernstein J: Other cystic kidney diseases. In: *Comprehensive Clinical Nephrology*, edited by Johnson R, Feehally J, Mosby International, London, 2003, pp 611–626
25. Sen S, Churchill GA: A statistical framework for quantitative trait mapping. *Genetics* 159: 371–387, 2001
26. Churchill G, Doerge R: Empirical threshold values for quantitative trait mapping. *Genetics* 138: 963–971, 1994
27. Irizarry R, Bolstad B, Collin F, Cope L, Hobbs B, Speed T: NARF: Summaries of Affymetrix GeneChip probe level data. *Nucleic Acids Res* 31: e15, 2003
28. Cui X, Churchill G: Statistical tests for differential expression in cDNA microarray experiments. *Genome Biol* 4: 210, 2003
29. Wu G, Tian X, Nashimura S, Markowitz G, Agati V, Park J, Yao L, Li L, Geng L, Zhao H, Edelmann W, Somlo S: Trans-heterozygous Pkd1 and Pkd2 mutations modify expression of polycystic kidney disease. *Hum Mol Gen* 11: 1845–1854, 2002

30. Storey J: A direct approach to false discovery rates. *J R Stat Soc B* 64: 479–498, 2002
31. Storey J, Tibshirani R: Statistical significance for genome-wide studies. *Proc Natl Acad Sci U S A* 100: 9440–9445, 2003
32. Vandesompele J, Preter KD, Pattyn F, Poppe B, Roy NV, Paepe AD, Speleman F: Accurate normalization of real-time quantitative RT-PCR data by geometric averaging of multiple internal control genes. *Genome Biol* 3: 0034.I–0034.II, 2002
33. Chapman A, Guay-Woodford L, Grantham J, Torres V, Bae K, Baumgarten D, Kenney PJ, King BF Jr, Glockner J, Wetzel L, Brummer ME, O'Neill WC, Robbin ML, Bennett WM, Klahr S, Hirschman GH, Kimmel PL, Thompson PA, Miller JP: Renal structure in early autosomal-dominant polycystic kidney disease (ADPKD): The Consortium for Radiologic Imaging Studies of Polycystic Kidney Disease (CRISP) cohort. *Kidney Int* 64: 1035–1045, 2003
34. Gilbert H, Le Roy P: Comparison of three multitrait methods for QTL detection. *Genet Sel Evol* 35: 281–304, 2003
35. Aitman T, Glazier A, Wallace C, Cooper L, Norsworthy P, Wahid F, Al-Majali K, Trembling P, Mann C, Shoulders C, Graf D, St Lezin E, Kurtz TW, Kren V, Pravenec M, Ibrahimi A, Abumrad NA, Stanton LW, Scott J: Identification of Cd36 (Fat) as an insulin-resistance gene causing defective fatty acid and glucose metabolism in hypertensive rats. *Nat Genet* 21: 76–83, 1999
36. Karp C, Grupe A, Schadt E, Ewart S, Keane-Moore M, Cuomo P, Kohl J, Wahl L, Kuperman D, Germer S, Aud D, Peltz G, Wills-Karp M: Identification of complement factor 5 as a susceptibility locus for experimental allergic asthma. *Nat Immunol* 1: 221–226, 2000
37. Wang X, Korstanje R, Higgins D, Paigen B: Haplotype analysis in multiple crosses to identify a QTL gene. *Genome Res* 14: 1767–1772, 2004
38. Miller M, Kumar S: Understanding human disease mutations through the use of interspecific genetic variation. *Hum Mol Genet* 21: 2319–2328, 2001
39. Chabardes-Garonne D, Mejean A, Aude J, Cheval L, Stefano AD, Gaillard M, Imbert-Teboul M, Wittner M, Balian C, Anthouard V, Robert C, Segurens B, Wincker P, Weissenbach J, Doucet A, Elalouf JM: A panoramic view of gene expression in the human kidney. *Proc Natl Acad Sci U S A* 100: 13710–13715, 2003
41. Cheverud JM, Routman EJ, Duarte FA, van Swinderen B, Cothran K, Perel C: Quantitative trait loci for murine growth. *Genetics* 142: 1305–1319, 1996
42. Masyuk TV, Huang BQ, Ward CJ, Masyuk AI, Yuan D, Splinter PL, Punyashthiti R, Ritman EL, Torres VE, Harris PC, LaRusso NF: Defects in cholangiocyte fibrocystin expression and ciliary structure in the PCK rat. *Gastroenterology* 125: 1303–1310, 2003
43. Kashtan C, Primack W, Kainer G, Rosenberg A, McDonald R, Warady B: Recurrent bacteremia with enteric pathogens in recessive polycystic kidney disease. *Pediatr Nephrol* 13: 678–682, 1999
44. Frisch M, Quint M, Lubberstedt T, Melchinger A: Duplicate marker loci can result in incorrect locus orders on linkage maps. *Theor Appl Genet* 109: 305–316, 2004
45. Abiola O, Angel JM, Avner P, Bachmanov AA, Belknap JK, Bennett B, Blankenhorn EP, Blizard DA, Bolivar V, Brockmann GA, Buck KJ, Bureau JF, Casley WL, Chesler EJ, Cheverud JM, Churchill GA, Cook M, Crabbe JC, Crusio WE, Darvasi A, de Haan G, Dermant P, Doerge RW, Elliot RW, Farber CR, Flaherty L, Flint J, Gershenfeld H, Gibson JP, Gu J, Gu W, Himmelbauer H, Hitzemann R, Hsu HC, Hunter K, Iraqi FF, Jansen RC, Johnson TE, Jones BC, Kempermann G, Lammert F, Lu L, Manly KF, Matthews DB, Medrano JF, Mehrabian M, Mittlemann G, Mock BA, Mogil JS, Montagutelli X, Morahan G, Mountz JD, Nagase H, Nowakowski RS, O'Hara BF, Osadchuk AV, Paigen B, Palmer AA, Peirce JL, Pomp D, Rosemann M, Rosen GD, Schalkwyk LC, Seltzer Z, Settle S, Shimomura K, Shou S, Sikela JM, Siracusa LD, Spearow JL, Teuscher C, Threadgill DW, Toth LA, Toye AA, Vadasz C, Van Zant G, Wakeland E, Williams RW, Zhang HG, Zou F; Complex Trait Consortium: The nature and identification of quantitative trait loci: A community's view. *Nat Rev Genet* 4: 911–916, 2003
46. Vale RD, Reese TS, Sheetz MP: Identification of a novel force-generating protein, kinesin, involved in microtubule-based motility. *Cell* 42: 39–50, 1985
47. Shipley K, Hekmat-Nejad M, Turner J, Moores C, Anderson R, Milligan R, Sakowicz R, Fletterick R: Structure of a kinesin microtubule depolymerization machine. *EMBO J* 23: 1422–1432, 2004
48. Woo D, Miao S, Pelayo J, Woolf A: Taxol inhibits progression of congenital polycystic kidney disease. *Nature* 368: 750–753, 1994
49. Woo D, Tabancay A, Wang C: Microtubule activate taxanes inhibit polycystic kidney disease progression in cpk mice. *Kidney Int* 51: 1613–1618, 1997
50. Miki H, Setou M, Hirokawa N: Kinesin superfamily proteins (KIFs) in the mouse transcriptome. *Genome Res* 13: 1455–1465, 2003
51. Lin F, Hiesberger T, Cordes K, Sinclair A, Goldstein L, Somlo S, Igarashi P: Kidney-specific inactivation of the KIF3A subunit of kinesin-II inhibits renal ciliogenesis and produces polycystic kidney disease. *Proc Natl Acad Sci U S A* 100: 5286–5291, 2003
52. Otto E, Schermer B, Obara T, O'Toole J, Hiller K, Mueller A, Ruf R, Hoefele J, Beekmann F, Landau D, Foreman JW, Goodship JA, Strachan T, Kispert A, Wolf MT, Gagnadoux MF, Nivet H, Antignac C, Walz G, Drummond IA, Benzing T, Hildebrandt F: Mutations in INVS encoding inversin cause nephronophthisis type 2, linking renal cystic disease to the function of primary cilia and left-right axis determination. *Nat Genet* 34: 413–420, 2003
53. Nurnberger J, Bacallao R, Phillips C: Inversin forms a complex with catenins and N-cadherin in polarized epithelial cells. *Mol Biol Cell* 13: 3096–3106, 2002
54. Morgan D, Eley L, Sayer J, Strachan T, Yates L, Craighead A, Goodship J: Expression analyses and interaction with the anaphase promoting complex protein Apc2 suggest a role for inversin in primary cilia and involvement in the cell cycle. *Hum Mol Genet* 11: 3345–3350, 2002